17th International Conference on Environmental Science and Technology

Athens, Greece, 1 to 4 September 2021

Kinetics study of the MO adsorption and photocatalytic degradation using an effectively engineered HF photocatalyst

THEODORAKOPOULOS G.[1,2,*], KATSAROS F.[2], PAPAGEORGIOU S.[2] and ROMANOS G.[2]

[1]School of Chemical Engineering, National Technical University of Athens, 9 Heroon Polytechniou Street, 15780 Zografou, Athens, Greece

[2]Institute of Nanoscience and Nanotechnology, N.C.S.R. "Demokritos", 15310 Ag. Paraskevi, Athens, Greece

*corresponding author: George V. Theodorakopoulos
e-mail: g.theodorakopoulos@inn.demokritos.gr

Abstract. In this study, copper decorated photocatalysts (Degussa P25), were shaped in the form of ceramic hollow fibers (HFs) and their photocatalytic properties were investigated using Methyl Orange (MO), a prototype anionic pollutant. The abatement of the dye was tested in dark and under UV irradiation by means of batch experiments and a possible mechanism was proposed for the MO photodegradation.

The photocatalysts were subjected to a series of MO adsorption experiments at variable initial concentrations, while the adsorption data were interpreted using different models. In general, the data analysis implied favorable MO physisorption on photocatalyst under the conditions used in this work. Furthermore, the adsorption kinetics of the photocatalysts was studied using pseudo-first and pseudo-second order kinetic equations, as well as Bangham, Elovich and Weber-Morris kinetic models. For further elucidation of the photocatalytic mechanism, experiments were performed with either O_2 or inert gas sparged MO solutions. It was concluded that the MO degradation rate followed the Langmuir-Hinshelwood (L-H) model.

In order to explore the stability of the derived ceramic HFs, their photocatalytic efficiency was investigated in successive cycles of batch photocatalytic experiments. Finally, a simple regeneration process revealed that the efficient photocatalysts could be reused without severe deactivation of their performance.

Keywords: Adsorption; Photocatalysis; Kinetics study; Batch reactor; MO degradation

1. Introduction

The use of photocatalysts in powder form has been related to several problems, including the difficult separation of the photocatalyst from the treated effluent and the non-effective irradiation of the dispersed particles in the photocatalytic slurry (Jawad et al., 2016), increasing significantly the operational and capital costs due to the use of high power UV sources, powerful agitation and processes for the effective separation for photocatalyst's retrieval downstream. Recent studies focus on the effective stabilization of the photocatalysts by embedding the photocatalytic particles into the matrix of polymers, predominantly structured in the form of fibers and beads.

In our recent work (Theodorakopoulos et al, 2021), the MO adsorption isotherms and kinetics of a Cu-decorated photocatalyst in HF form were explored for defining the correlation between the physicochemical properties of HFs and their adsorption performance.

Since an additional target of this work was to elucidate the role of O_2, both in scavenging the photogenerated electrons and in forming active oxygen radicals, adsorption tests with O_2-depleted and O_2-saturated solutions were also conducted. In doing so, we were able to assess whether the beneficial or adverse effects of dissolved O_2 in photocatalysis could be attributed solely to its role as a scavenger or if it also affects pollutant adsorption, potentially having a significant synergetic impact on photocatalytic efficiency. Finally, we explored the models' adsorption parameters in order to shed light onto the adsorption mechanism pathway and to investigate the photocatalyst capacities, whilst effectively designing the photocatalytic system and select the best model to fit the experimental kinetic curves.

2. MO adsorption capacity

2.1. MO adsorption kinetics

Amongst the several examined models, the pseudo-second order model and those of Bangham and Weber-Morris were found to describe better the kinetics of MO uptake onto HFs. The initial adsorption rate (h, mg/g·min) increased with the adsorbate concentration indicating that more MO molecules reached the adsorbent's surface within a short period of time, due to a greater driving force for mass transfer. The linearity of the Bangham plots for all studied MO concentrations leads to the conclusion that MO adsorption kinetics is limited by pore diffusion of MO uptake onto HFs (Tütem et al., 1998). Same conclusion was extracted via analysis with the Weber-Morris model (plot crossing through the axis origin). Indeed, it is concluded that intraparticle diffusion controls the MO uptake process except from the

case of the higher initial MO concentration (24 ppm), where a boundary layer diffusion mechanism seems to control the MO adsorption.

2.2. MO adsorption on O_2-saturated dye solutions

Cu-decorated HFs MO adsorption capacity was found to be 2.3 mg/g at a concentration of 6.3 ppm. As already shown in our previous work, decoration of HFs with zero-valent copper and copper oxide nanoparticles resulted in enhanced pore structural and surface texture characteristics. Additionally, copper nanoparticles enhanced the photocatalytic process acting either as a sink for the photogenerated electrons (metallic copper) or forming p–n CuO/TiO_2 heterojunctions, improving the electron-hole separation. Furthermore, the reductive activity of zero-valent copper towards the cleavage of the azo-group of several dyes should be also taken into account. Zero-valent copper nanoparticles, though not efficient adsorbents for MO (Li et al., 2015), still have the capacity, as efficient electron donors, to transfer electrons to the dye, promoting the reductive cleavage of the azo group even in the absence of UV irradiation (Cao et al., 1999; Nam and Tratnyek, 2000). Therefore, in Cu-decorated HFs both the enhanced pore structural characteristics and the reductive action of the Cu nanoparticles are responsible for the outstanding MO removal. In this context, Cu-decorated HFs were selected, as the most promising, to be further studied at variable MO initial concentrations. For a solid-liquid system, the adsorption isotherm is a significant physicochemical descriptor of adsorption behavior and can provide valuable information on the surface properties of the catalyst. In this work, five renowned isothermal models, Langmuir, Freundlich, Sips, Temkin and Dubinin-Radushkevich (D-R), were applied to the experimental data. In general, the models fitting results imply favorable physisorption of MO on the studied sample under the conditions used with the Sips and Freundlich isotherm models providing the best fit. As a remark, Sips model is reduced to the Langmuir equation, indicating a material with relatively homogenous binding sites.

2.3. MO adsorption on O_2-depleted MO solutions

In the case of O_2-depleted MO solution (6.3 ppm), an almost similar adsorption capacity (2.28 mg/g) is determined for the Cu-decorated HFs. In addition, the HFs were subjected to a series of MO adsorption experiments at variable initial concentrations, to make possible the interpretation of adsorption data with the aforementioned adsorption isotherm models. The values of exponent n (1.03) of the Freundlich model and of the mean free energy E (0.689 kJ/mol) of the D-R model are in the range of a favorable adsorption and of a physisorption process, respectively. The higher values of R^2 for D-R isotherm indicate that the equilibrium adsorption data fit better with this model.

3. Evaluation and reaction kinetics of HFs

3.1. O_2-saturated solution-First Experimental Cycle

The aqueous MO solution was sparged with O_2 prior to each photocatalytic run. Total kinetics of MO degradation at the examined concentrations and indicative plot of the attenuation of the main (464 nm) and secondary (271 nm) MO absorbance peak during the photocatalytic process with the Cu-decorated HFs are presented in Figure 1a. The attenuation of the MO absorbance peaks at λ = 464 and 271 nm in inset of Figure 1a indicates a rapid degradation of the azo dye. The secondary peak attenuates significantly after 90 min of UV illumination, suggesting the destruction of the aromatic ring. It is also noteworthy to observe that there is a blue shift of the main peak (464 nm) throughout the photodegradation process. This indicates that after the reductive cleavage of the azo group through the mechanism implied by the zero-valent copper, certain modifications may occur on the chemical groups of the two produced molecules (Chen et al., 2008).

On the other hand, it has often been observed that the rate of photocatalytic degradation of several dyes follows the Langmuir-Hinshelwood (L-H) model (Papageorgiou et al., 2012). For a millimolar solution concentration, pseudo-first order kinetics was assumed in order to calculate the corresponding degradation rate constant k_{app} (min^{-1}):

$$In(C_0/C) = k_r \cdot K_{LH} \cdot t = k_{app} \cdot t,$$

where C_0, is the initial concentration in mg/L, C, is the concentration (mg/L) at a given time t (min), k_r, is the reaction rate constant (mg/L·min) and K_{LH}, the adsorption constant of the reactant (L/mg). As such, the initial degradation rate can be derived from the following equation:

$$r' = k_{app} \cdot C_0$$

A plot of $ln(C_0/C)$ versus time for the examined initial concentrations is presented in Figure 1b. The linear regression slope equals to the k_{app} rate constant. Comparing between the kinetic data calculated from the main and secondary UV absorbance peaks for MO, the catalytic photodegradation process was more efficient in breaking the azo bond than the aromatic ring, thus confirming the dominant role of zero-valent copper nanoparticles in promoting the reductive cleavage of the chromophore.

Moreover, the linear form of the L-H model represented by the following equation, expresses the dependence of $1/r'$ values on the respective $1/C_0$ values:

$$1/r' = 1/k_r + 1/k_r K_{LH} \cdot 1/C_0$$

The k_ro and K_{LH}o values calculated from the slope and intercept were 0.104 mg/L/min and 0.093 L/mg, respectively. According to the L-H model, identical values of K_{LH} and the Langmuir adsorption constant (b = 0.094 L/mg) confirm the dye's affinity to the catalytic surface.

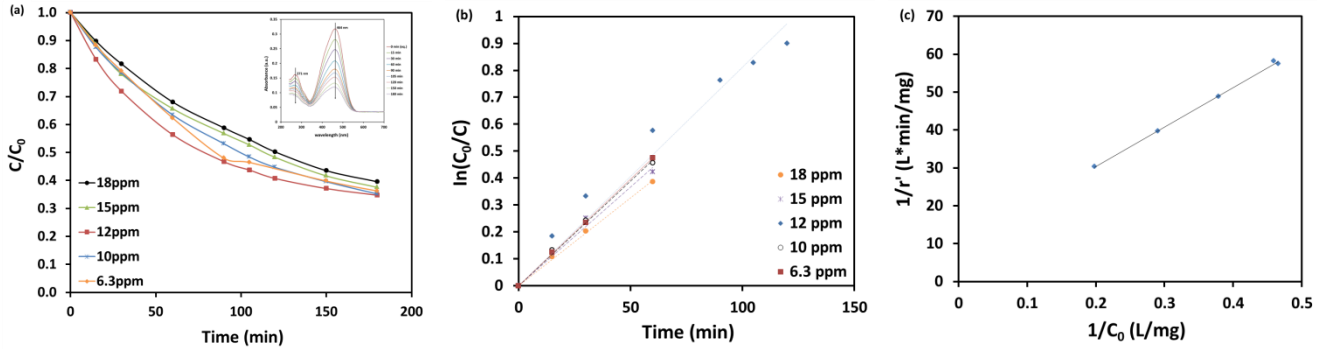

Figure 1. (a) Total kinetics of MO degradation in O_2-saturated solutions at the examined concentrations for HFs. In the inset, indicative plot of the reduction of the main and secondary MO absorbance peaks during the photocatalytic process at C = 15 ppm is presented. (b) Linear transform $\ln(C_0/C) = f(t)$ of the MO disappearance (c) Linear fit of the data to the L-H model from Figure 1b

3.2. O_2-depleted solution-First Experimental Cycle

Similar procedure was applied for the HFs in order to study the reaction kinetics in the O_2-depleted MO solution. Comparison of the MO degradation k_{app} values of the O_2-depleted and O_2-saturated solutions shows they are almost identical. Despite the fact that the Cu-decorated HFs adsorption capacity towards MO was degraded in the O_2-saturated solution and although dissolved O_2 can act as a scavenger for the photogenerated electrons (generating $\cdot O_2^-$, instead of the very drastic $\cdot$OH radicals), the photocatalytic efficiency of the sample remained unaffected. This result implies that the major mechanism behind the enhanced MO degradation capacity is the reductive cleavage of the azo group.

Again, in this case, the k_ri and K_{LH}i values were calculated at 0.057 mg/L/min and 0.200 L/mg, respectively. The values of K_{LH} and b (0.055 L/mg) deviate suggesting that the reaction occurs not only at the surface, but also in the bulk solution entrapped within the pore structure of the HFs.

In order to estimate the reaction rate of first order kinetics, one of the most practical indicators is the calculation of the half-life time of reaction. At the half-life time of reaction ($C = 0.5 \cdot C_0$), the reaction time $t_{1/2}$ is calculated by the following equation:

$$t_{1/2} = 0.5 \cdot C_0/k_r + \ln 2/k_r \cdot K_{LH}$$

Additionally, for reactions exhibiting pseudo-first order kinetics, the half-life time can be derived from the following equation:

$$t'_{1/2} = \ln 2/k_{app}$$

The assessment of these values showed, in general, a difference between $t_{1/2}$ and $t'_{1/2}$, which became significant with increasing initial MO concentration. This trend, which was smoother in the case of the O_2-saturated solution, could be interpreted on the grounds of the formation of intermediates that could be adsorbed competitively on the catalyst causing retardation of the kinetics. Thus, as a general comment for the kinetic model study, the competition of the intermediate byproducts during the photocatalytic process should be considered.

3.3. Stability of the photocatalytic performance

In Table 1 we present, in comparison, the MO rejection performance between a fresh sample and a sample subjected to four successive experimental cycles. There seems to exist a concentration threshold (12 ppm of MO), above which, the rejection efficiency during the fourth photocatalytic cycle appears severely degraded. Furthermore, the sample preserves the half values of rejection until the 15 ppm concentration, while, at the highest concentration studied, it retains approximately 40% of the initial performance. It can also be concluded that the concentration thresholds for a severe degradation of the photocatalytic and adsorption performances coincide. This highlights the important contribution of adsorption in photocatalysis. Moreover, beyond this threshold, all the active sites for adsorption on the sample are occupied (saturation), and lack of effective regeneration with simple washing has as result the severe degradation of adsorption and photocatalytic performance.

In the case of the O_2-depleted solution, the total kinetics of MO degradation at the studied concentrations is also presented in Table 1, where the MO rejections after four experimental cycles for the MO absorbance peak are compared to the initial rejections (values in parentheses from the first run). Comparing the data in Table 1, a concentration threshold (15 ppm) seems to exist, over which the photocatalytic and adsorption performance severely decreases. In the O_2-depleted solution, more active adsorption sites on the sample are available, compared to the O_2-saturated one, as the dissolved O_2 acting as a scavenger occupies residual carbon sites.

Table 1. MO rejection (%) for the studied concentrations compared to the first run (values in parentheses)

$C_{initial}$ (ppm)	R_o (%)	R_i (%)
6.3	61.5 (62.3)	63.0 (72.4)
10	53.7 (64.8)	52.1 (51.0)
12	60.7 (65.3)	-
15	33.0 (62.5)	29.5 (61.7)
18	15.9 (60.5)	9.4 (39.2)
24	18.7 (44.2)	-

In addition to the photocatalytic efficiency, the mechanical stability and resistance to attrition of the HFs was examined under the experimental conditions (vigorous stirring for long periods of time). Thus, fresh sample was weighed before each photocatalytic test and reweighed following completion of the next photocatalytic cycle after drying, in order for mass losses via attrition to be calculated. The overall weight loss was minor (1.2%) verifying the good mechanical properties of the HFs. Consequently, it is confirmed that during each photocatalytic/regeneration cycle, a carbonaceous phase endows the sintered TiO_2 nanoparticles with enhanced resistance to attrition under the conditions of vigorous stirring.

4. Conclusions

In this work, the pseudo-second order, Bangham and Weber-Morris models were found to describe better MO adsorption onto the Cu-decorated HFs, suggesting more than one mechanism involved in the MO uptake onto HFs. Sips, Freundlich and D-R isotherms fit well with the equilibrium adsorption data, whilst the MO degradation rate followed the Langmuir-Hinshelwood (L-H) model indicating that the competition of the intermediate byproducts during the photocatalytic process is an important factor to be considered.

Copper nanoparticles were found to act as a sink for the photogenerated electrons, thus benefiting the photocatalytic process due to avoidance of electron/hole recombination and on the other hand, they effectively shuttle electrons to the MO molecules. Furthermore, copper nanoparticles contribute to the photocatalytic process by promoting the second route of ˙OH generation, involving the photogenerated electrons from the conduction band that initially react with the adsorbed oxygen to produce oxygen radicals and hydrogen peroxide which, in turn, reacts to form ˙OH radicals.

Finally, the structured Cu-decorated photocatalysts exhibit good mechanical stability and resistance to attrition, while they retain their high activity for at least four cycles at moderate initial MO concentrations up to 12 ppm making them a good candidate for dynamic flow experiments and validating the feasibility of their use in continuous flow industrial processes.

References

Cao J., Wei L., Huang Q., Wang L. and Han S. (2016), Reducing degradation of azo dye by zero-valent iron in aqueous solution, *Chemosphere*, **38**, 565-571.

Chen T., Zheng Y., Lin J.-M. and Chen G. (2008), Study on the photocatalytic degradation of methyl orange in water using Ag/ZnO as catalyst by liquid chromatography electrospray ionization ion-trap mass spectrometry, *Journal of the American Society for Mass Spectrometry*, **19**, 997-1003.

Jawad A.H., Mubarak N.S.A., Ishak M.AM., Ismail K. and Nawawi W.I. (2016), Kinetics of photocatalytic decolourization of cationic dye using porous TiO_2 film, *Journal of Taibah University for Science*, **10**, 352-362.

Li P., Song Y., Wang S., Tao Z., Yu S. and Liu Y. (2015), Enhanced decolorization of methyl orange using zero-valent copper nanoparticles under assistance of hydrodynamic cavitation, *Ultrasonics Sonochemistry*, **22**, 132-138.

Nam S. and Tratnyek P.G. (2000), Reduction of azo dyes with zero-valent iron, *Water Research*, **34**, 1837-1845.

Papageorgiou S.K., Katsaros F.K., Favvas E.P., Romanos G.Em., Athanasekou C.P., Beltsios K.G., Tzialla O.I. and Falaras P. (2012), Alginate fibers as photocatalyst immobilizing agents applied in hybrid photocatalytic/ultrafiltration water treatment processes, *Water Research*, **46**, 1858-1872.

Theodorakopoulos G.V., Romanos G.Em., Katsaros F.K., Papageorgiou S.K., Kontos A.G., Spyrou K., Beazi-Katsioti M. and Falaras P. (2021), Structuring efficient photocatalysts into bespoke fiber shaped systems for applied water treatment, *Chemosphere*, **277**, 130253.

Tütem E., Apak R. and Ünal Ç.F. (1998), Adsorptive removal of chlorophenols from water by bituminous shale, *Water Research*, **32**, 2315-2324.